Journal of ELECTRONIC MATERIALS, Vol. 37, No. 9, 2008
DOI: 10.1007/s11664-008-0447-y
© 2008 TMS
Special Issue Paper

Defects in HgTe and CdHgTe Grown by Molecular Beam Epitaxy

E. SELVIG,[1,2] C.R. TONHEIM,[1] T. LORENTZEN,[1] K.O. KONGSHAUG,[1]
T. SKAULI,[1] and R. HAAKENAASEN[1]

1.—Norwegian Defence Research Establishment, P.O. Box 25, NO-2027 Kjeller, Norway.
2.—e-mail: espen.selvig@ffi.no

The defect morphology in HgTe and CdHgTe was studied in (211)B-oriented layers grown in a 20°C temperature range around the optimal growth temperature. The density of defects varies strongly with the growth temperature. In HgTe, the shape of the microvoid defects is very sensitive to the growth temperature and can be used to determine the deviation from the optimal growth temperature. Using thermodynamical modeling, the optimal growth temperature for CdHgTe can then be calculated. We describe a mechanism for the formation of microvoids and needles which involves preferential surface diffusion of Te combined with an impurity or defect on the substrate. Microvoids on (111)B-oriented partially twinned HgTe layers were also studied. The microvoids in the twinned parts of the layer were found to be rotated 180 deg relative to the untwinned parts of the layer.

Key words: CdHgTe, HgCdTe, HgTe, molecular beam epitaxy, defects, voids, microvoids, needles, photoluminescence, X-ray diffraction

INTRODUCTION

CdHgTe is an important material for infrared detectors[1,2] as the direct band gap can be compositionally tuned from −0.26 eV to 1.61 eV at 77 K.[3] Defects in CdHgTe can be detrimental to detector performance,[4,5] and it is therefore important to optimize the growth conditions to reduce their density. To this end we have performed a study of defects in the CdHgTe material system to determine how the different defects relate to the growth conditions. A study of the defects in HgTe has also been performed because HgTe is a simpler material system than CdHgTe, but presents similar challenges as CdHgTe with respect to crystalline quality. Thus, the results obtained from the HgTe study can help us understand defect formation in the more complicated CdHgTe material.

CdHgTe and HgTe layers grown on (211)B-oriented CdZnTe substrates were grown at different growth temperatures in a range of around 20°C around the optimal growth temperature. We present the variation of defect density and defect morphology with temperature and find that the optimal growth temperature for both HgTe and CdHgTe is just below the onset of Te precipitation (Te-phase limit). Furthermore, we show that in HgTe the deviation from the optimal growth temperature can be determined from the shape and clustering of the microvoids, whereas this is not possible for CdHgTe. However, when the Te-phase limit has been found for HgTe, the Te-phase limit in $Cd_xHg_{1-x}Te$ for x within the range 0 to 0.50, and thereby the optimal growth temperature, can be calculated using thermodynamics.

Furthermore, we have performed a study of photoluminescence (PL) of (211)B-oriented CdHgTe layers with growth temperature and a study of microvoid defects in a partially twinned (111)B-oriented HgTe layer.

EXPERIMENTAL

Molecular beam epitaxial (MBE) growth of 3-μm-thick HgTe and $Cd_xHg_{1-x}Te$ layers was performed on 7.5 mm × 7.5 mm (211)B-oriented CdZnTe substrates (wire-sawn from 15 mm × 15 mm substrates).

(Received November 28, 2007; accepted March 10, 2008; published online April 9, 2008)

Details of the substrate preparation and effusion cells were described in a previous publication.[6] The Hg flux was kept constant for all layers (8.50×10^{20} m^{-2} s^{-1}). For the CdHgTe layers the growth temperature was varied over a 21°C range. The CdHgTe growth rate was 540 ± 90 Å min^{-1}. The CdHgTe layers were capped with an 18 Å CdTe layer to avoid surface decomposition during cool-down. For the HgTe layers the growth temperature was varied over an 18°C range. The growth temperature throughout the layer was constant. The nominal HgTe growth rate was 500 Å min^{-1}. After growth of the HgTe layers the heaters of the substrate and the Hg cell were switched off simultaneously so that the epilayers were cooled down in a decreasing Hg flux to avoid surface decomposition.

Some 3-μm-thick HgTe and CdHgTe layers were also grown on uncut 15 mm × 15 mm (211)B-oriented CdZnTe substrates at a growth temperature close to the optimal growth temperature. A 3-μm-thick HgTe layer was grown on an uncut 10 mm × 10 mm (111)B-oriented CdZnTe substrate.

Good control of the growth temperature is important. We use a Ga-wetted thermocouple for good control of the substrate temperature.[7] To ensure that the temperature measurement system did not drift, In melting point measurements were performed prior to, during, and after growth of the series of layers described above. The maximum deviation between the measured In melting point temperatures was 1.5°C, which is approximately three times the uncertainty in the melting point measurement. This shows that there was little drift in the growth temperature measurement system over the period when the layers were grown.

Transmission spectroscopy was used to determine the composition and thickness of the CdHgTe layers. Other characterization techniques used were optical microscopy, atomic force microscopy (AFM), scanning electron microscopy (SEM) with energy dispersive X-ray spectroscopy (EDX), transmission spectroscopy, high-resolution X-ray diffraction (HRXRD), and PL. A Fourier-transform infrared spectrometer (FTIR) was used for transmission spectroscopy and PL measurements.

In HRXRD the 422 and 533 reflections, as well as the 533 twin reflection, were measured for the (211)B-oriented layers. The twin content was measured by dividing the integrated intensity of the 533 twin reflection by the sum of the integrated intensities of the 533 reflection and the 533 twin reflection.

Defects were counted by recording up to nine micrographs (each image covering an area of 80 μm × 110 μm) and counting the defects manually. The actual number of images used for a particular sample was chosen according to the defect density to ensure good counting statistics. For counting of the larger high-temperature voids, images with smaller magnification (430 μm × 580 μm) were recorded. We have also performed an etch-pit density (EPD) measurement using the Hähnert and Schenk[8] etch. PL was measured from the CdHgTe layers at 11 K using an excitation laser emitting at 2.01 μm with an intensity of 3.2 W cm^{-2}.

We define the optimal growth temperature (T_{opt}) as the temperature at which the area covered by defects is minimized. We will conclude below that T_{opt} is 193.3°C for HgTe with the Hg flux used in our experiments. For simplicity we will give all temperatures in the discussion as a deviation in degrees Celsius from T_{opt}.

RESULTS AND DISCUSSION

(211)B HgTe Surface Morphology

There is a clear trend in the HgTe microvoid shape and density as the temperature is varied. Microvoids in layers grown at different growth temperatures are shown in Fig. 1. Microvoids form clusters at low temperatures (Fig. 1a and b). The number of microvoids in these clusters decreases as the temperature increases (five to nine microvoids at T_{opt} − 6°C and two to five microvoids at T_{opt} − 4°C) until they are single microvoids at T_{opt}. At T_{opt} the basic shape of the microvoid could be observed (Fig. 1c). It is an indented diamond with a longer axis in the step-flow direction, $[1\bar{1}\bar{1}]$, and a shorter axis along the step direction, $[01\bar{1}]$. At the centre of the diamond there is a hole, and from this hole out along the long axis there is usually a canal extending all the way up to the film surface. The shape of the microvoids changes from diamond shaped to triangular as the temperature is increased, as explained in more detail below.

Above T_{opt} − 4°C the diamond becomes increasingly more truncated, and the remaining facets built up above the film surface give the defect a 'bat-like' appearance. At the optimal growth temperature, T_{opt}, no clustering occurs and the microvoids are all of bat-like shape (Fig. 1c). At higher temperatures the $(\bar{1}11)$ plane gradually truncates the diamond so that the microvoid becomes a triangle as the temperature is increased toward T_{opt} + 6°C (Fig. 1d). The shape and clustering of the microvoids can thus be used as an indicator of the growth temperature. Further details about the temperature dependence can be found in a previous publication.[6]

The walls of the microvoids are facetted. The length of the microvoids increases from ~0.5 μm to 1.2 μm in the temperature range T_{opt} − 4°C to T_{opt} + 4°C. Parts of the facets surrounding the microvoids form an elevation of 0.05 μm to 0.2 μm relative the (211) surface. This elevation is significantly larger on the step-flow direction side of the microvoid. EDX point spectra and line scans across microvoids in HgTe showed no difference between the composition in the microvoid and the surrounding layer.

Other defects were also observed in these layers. Large densities of hillocks were observed in layers grown from T_{opt} − 2°C to T_{opt} + 6°C with defect densities around 10^5 cm^{-2}.[6] There are large

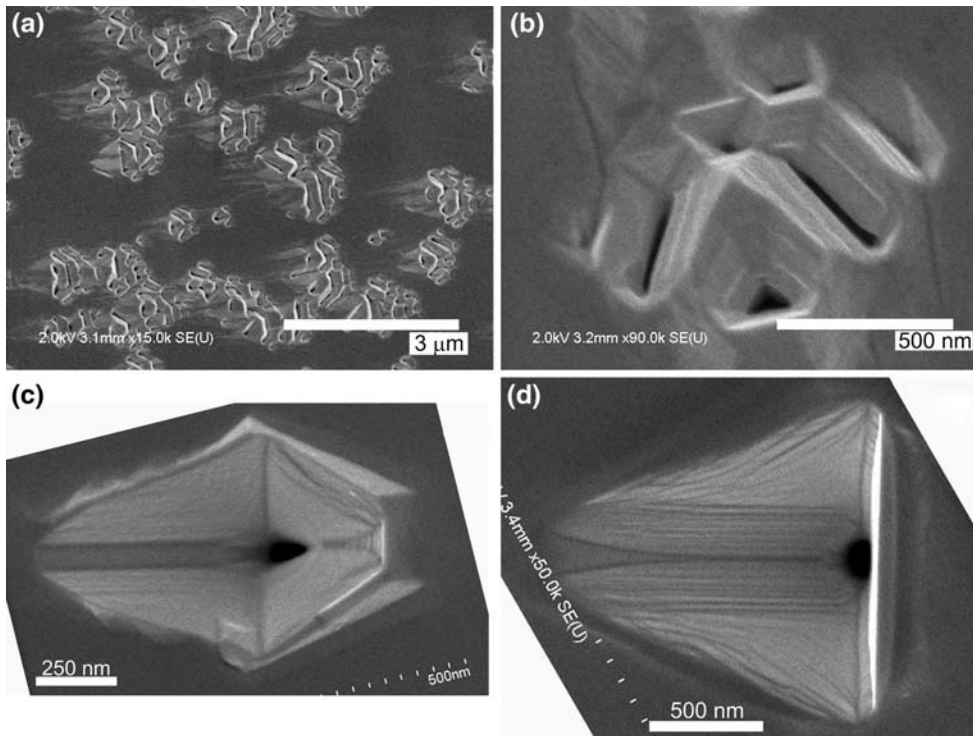

Fig. 1. Microvoids in HgTe layers grown at different growth temperatures. (a) T_{opt} – 10°C, (b) T_{opt} – 6°C, (c) T_{opt}, and (d) T_{opt} + 6°C. The step-flow direction is toward the right in panels (c) and (d).

uncertainties in the density of hillocks because they can be difficult to observe. Hillocks are therefore excluded from the calculation of the surface area covered with defects below. Furthermore they can be confused with surface morphology undulations. Large densities of circular voids which consist of a void in the centre of a plateau typically 4 nm to 10 nm high with a diameter 0.6 μm to 1.6 μm have been observed at $T_{opt} - 2°C$ and above. The void diameter is in the range of 0.35 μm to 0.60 μm.

High-temperature voids (also known as V-shaped defects,[9] surface crater voids,[10] and voids[11–13]) start forming when the growth temperature is increased above the Te-phase limit and Te precipitates are formed.[14,15] These voids contain Hg-deficient polycrystalline HgTe (Fig. 2).[6] The size of these voids increased from 2 μm to 100 μm as the growth temperature was increased from T_{opt} + 1°C to T_{opt} + 8°C.

The percentage of surface area covered by defects versus growth temperature is shown in Fig. 3. The calculation of the total defect area was based on the area and density of microvoids, circular voids, and high-temperature voids. The minimum area covered by defects is obtained at a growth temperature of 193.3°C, which is therefore the optimal growth temperature. This temperature is 1°C below the onset of high-temperature voids. The Te-phase limit is the lowest growth temperature where Te precipitation (resulting in high-temperature voids) occurs.

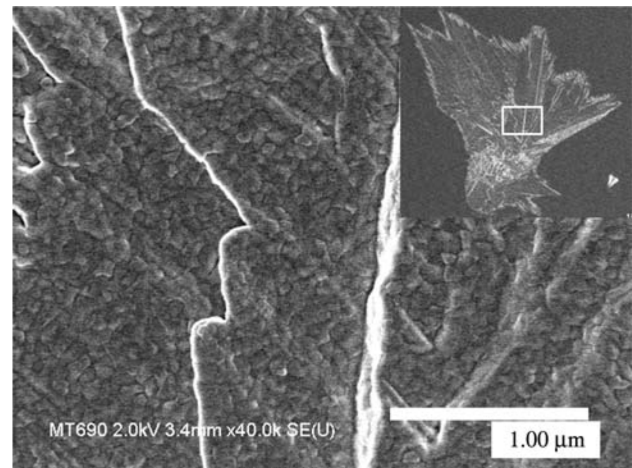

Fig. 2. SEM image of the interior of a high-temperature void in a HgTe layer grown at T_{opt} + 6°C. The whole high-temperature void is shown in the inset.

We have grown layers in 1°C to 2°C intervals around the Te-phase limit. This limits the accuracy of the experimentally determined Te-phase limit. In the discussion below we place the experimentally determined Te-phase limit at the lowest growth temperature where high-temperature voids are observed.

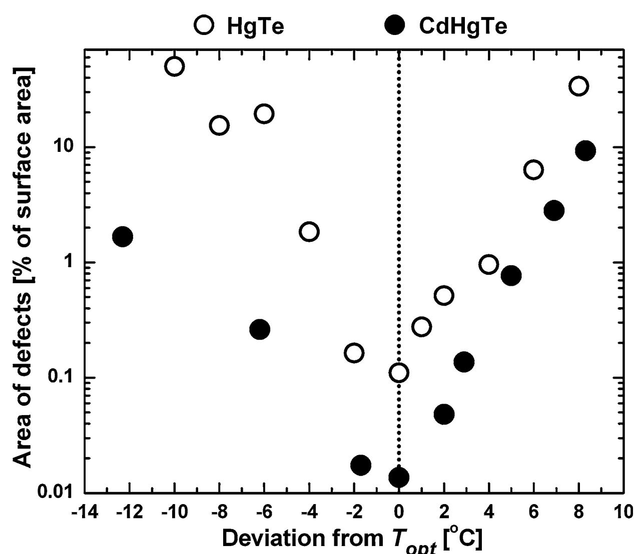

Fig. 3. Percentage of HgTe and CdHgTe surface area covered by defects versus growth temperature. The optimal growth temperature is indicated by the dotted line.

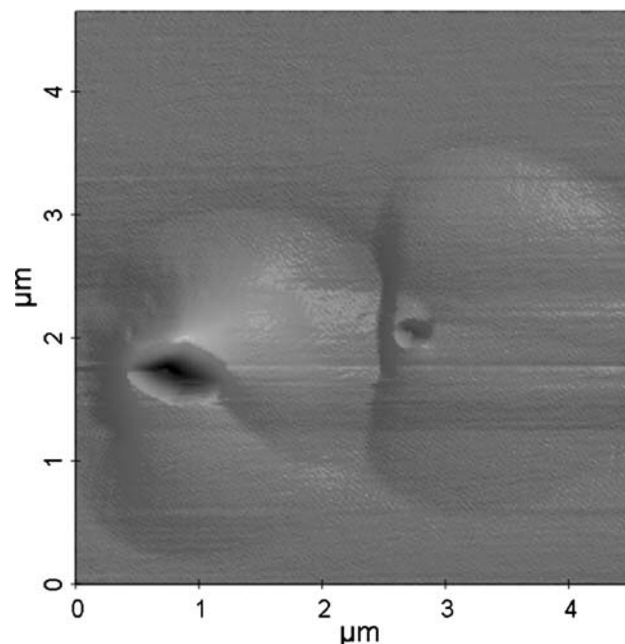

Fig. 5. AFM image of two hillock-with-void defects. The step-flow direction is toward the right.

(211)B CdHgTe Surface Morphology

The composition, x-value, of the $Cd_xHg_{1-x}Te$ layers lies in the range of 0.27 to 0.44. The microvoids in CdHgTe can be divided into two groups: facetted microvoids (Fig. 4) similar to the ones in HgTe, and the voids surrounded by a hillock (Fig. 5). The facetted microvoids are diamond shaped below T_{opt}, and are triangle shaped above T_{opt}.

There are microvoids of many different sizes and shapes in the same layer. At the lowest growth temperature used for the CdHgTe series, T_{opt} – 12.3°C, the microvoids are mostly unclustered. Some clusters containing five microvoids were observed. Similar to in HgTe, there is a build-up around the facetted microvoids. The build-up is higher on the step-flow direction side of the microvoid. The microvoids in CdHgTe are generally more rounded than in HgTe.[16] At and above T_{opt} – 1.7°C the majority of the microvoids are surrounded by a hillock, and can be called hillocks-with-void (Fig. 5).[17] The shape of the voids in hillocks vary from diamond to round. A more in-depth description can be found in a previous publication.[16]

Above the Te-phase limit many of the microvoids contain polycrystalline CdHgTe (Fig. 6). These seem to be the beginning of high-temperature voids. This indicates that nucleation of high-temperature voids is facilitated on microvoids. Polycrystalline CdHgTe was not observed on all microvoids in the samples depicted in Fig. 6. Additionally, in the same samples we observed polycrystalline CdHgTe (high-temperature voids) where no microvoid features could be observed underneath, indicating that not all high-temperature voids nucleate on microvoids.

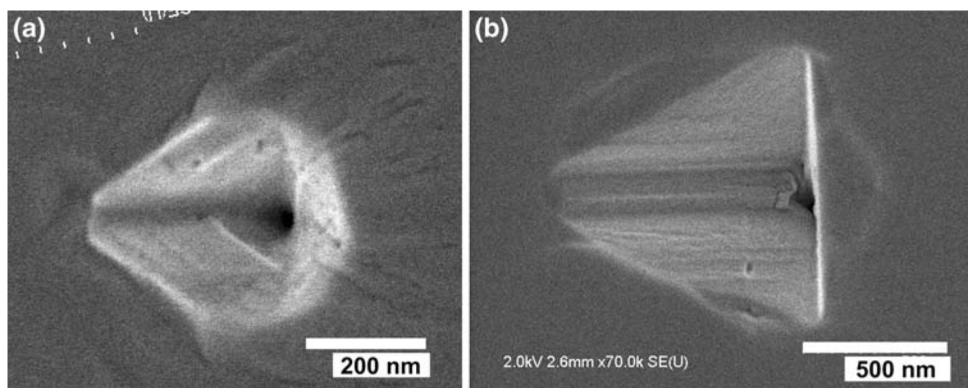

Fig. 4. Facetted microvoids in CdHgTe layers grown at different temperatures. (a) T_{opt} – 12.3°C and (b) T_{opt} + 2.9°C. The step-flow direction is toward the right.

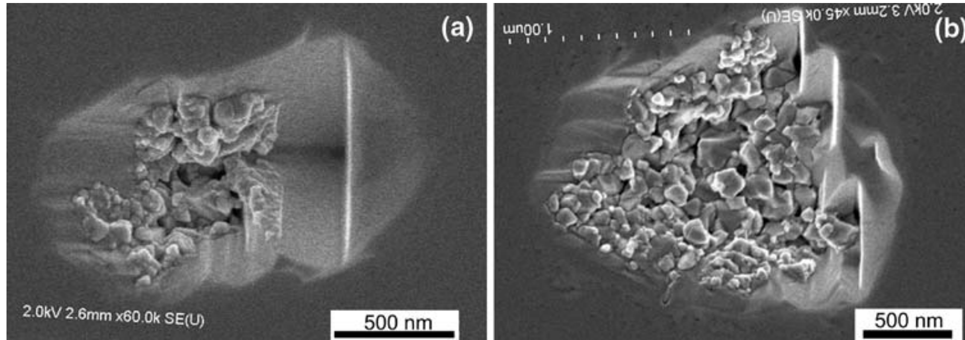

Fig. 6. Early stages of formation of a high-temperature void on a microvoid in CdHgTe. The growth temperatures were (a) T_{opt} + 2.9°C and (b) T_{opt} + 2°C. The step-flow direction is toward the right.

The average size of the high-temperature voids increased from 1 μm to 20 μm as the growth temperature was increased from T_{opt} + 2.0°C to T_{opt} + 8.3°C. Images of high-temperature voids from layers grown at different growth temperatures have been presented in a previous publication.[16]

Hillocks have also been observed in CdHgTe with densities in the range 1×10^5 cm^{-2} to 3×10^6 cm^{-2}.[16] There are uncertainties in the hillock densities because the hillocks can be hard to spot and are difficult to distinguish from undulations on the surface. The hillocks are therefore not included in the defect density plots.

In CdHgTe layers we have observed needle-shaped features aligned along the $[01\bar{1}]$ step direction. The needles consist of a ridge and a depression on the surface. From AFM profiles of needles we find that the inclined plane on the right side of the depression is the $(11\bar{1})$ plane.[16] Needles have not been observed in HgTe. We have not been able to associate needles with dislocations (through Hähnert and Schenk dislocation etch and XRD full width half maximum measurements, FWHM) or twinning around the [111] axis (through reflection high-energy electron diffraction (RHEED) observations, XRD twin reflection measurements, and etch pit studies).[18] Needle lengths were unaffected by defect etching. AFM volume calculations indicate that all the missing material in the depression is found in the ridge. It therefore seems that the needles are local height variations of CdHgTe with (almost) the same composition as the surrounding material. There are conflicting suggestions in the literature as to the origins of needles: twin-free faceting on the CdHgTe (211) surface,[19] substrate surface roughness,[20] or a high density of twins.[21] Similar needles have also been reported in SiC layers grown on (211)-oriented Si substrates, where they were associated with step bunching.[22] We believe the needles have been formed by preferential Te surface diffusion during growth, as explained in the next section.[18]

Defect densities are plotted versus temperature in Fig. 7. The surface area covered by defects versus growth temperature is plotted in Fig. 3. Again we define the optimal growth temperature (T_{opt}) as the growth temperature minimizing the total surface area covered by defects. Using this definition we find that the optimal growth temperature lies 2°C below the onset of high-temperature voids. However, due to the limited number of samples it is difficult to determine accurately where the minimum in surface coverage would have been if more samples had been grown. The true optimal substrate lies somewhere between T_{opt} − 1.7°C and T_{opt} + 2°C which is maximum 3.7°C from the Te-phase limit.

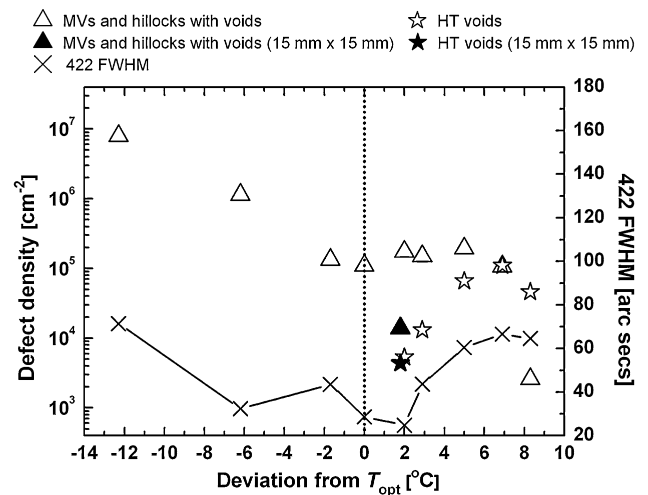

Fig. 7. Defect density and HRXRD 422 FWHM in CdHgTe layers plotted versus growth temperature. MVs = microvoids; HT voids = high-temperature voids. Note that the symbols for MVs and HT voids overlap at T_{opt} + 6.9°C. The optimal growth temperature is indicated by the dashed line.

The microvoid defect density (including the hillock-with-void density) decreased as the temperature was increased from T_{opt} − 12.3°C, stabilized in the temperature range T_{opt} − 1.7°C to T_{opt} + 6.9°C, and then fell significantly. In contrast, the microvoid defect density in HgTe fell continuously as the growth temperature increased.[6]

A 3-μm-thick $Cd_{0.34}Hg_{0.66}Te$ layer grown on a 15 mm × 15 mm uncut substrate at T_{opt} + 2 shows a factor of 13 lower microvoid density. We have previously reported a factor of 73 reduction in microvoid density on an uncut substrate.[6] However, smaller microvoids were found during a recount. When these were included a factor of 13 reduction in microvoid density is obtained on an uncut substrate. A factor of 11 decrease in microvoid defect density was observed on a HgTe layer grown on an uncut substrate versus a cut substrate. The high densities of defects in layers grown on the sawn substrates are probably due to either dust from the sawing or contamination from the wax or dissolving-cleaning agents used in the sawing process.[6] However, the highly varying microvoid density with temperature (more than two orders of magnitude) shows that the nucleation of the microvoids clearly depends on the growth conditions as well as on the substrate preparation.

The layer grown on the uncut substrate exhibited very good properties: 422 XRD FWHM of 22.9″, a PL FWHM of 7.5 meV at 11 K, and an EPD of 52500 cm^{-2} (as measured by Nomarski microscopy), which is close to the substrate EPD density specified by the supplier. Whereas the microvoid defect density was a factor of 13 lower than in the layers grown on sawn substrates, the high-temperature void defect density was similar in sawn and uncut substrates.

Formation of Microvoids and Needles in (211)B-oriented Layers

The mechanism for formation of facetted microvoids appears to be initiated by impurities or defects causing local blocking of the diffusion of Te atoms on the growing surface.[6,16] We have suggested that Te atoms diffuse preferentially in the $[\bar{1}11]$ direction on (211)B, whereas on a symmetric plane they will have no preferential diffusion direction. If an impurity on the surface is blocking the diffusion of Te atoms the result will be a build-up of material on the upstream side (step-flow-direction side) of the impurity. On the downstream side of the impurity there will be a deficiency of material, i.e., a void. The impurity could be Te_2 molecules incorporated on the surface.[23]

This model can also explain the needle-shaped morphology often observed in CdHgTe layers (Fig. 8).[18–21] The needles consist of a trench and a material build-up on one side of the trench. We have found that the density of needles is reduced after a bake-out of the growth chamber, but also that the density of needles are reduced if a few thin alternating layers of CdTe and CdHgTe are grown between the substrate and the thick CdHgTe layer. This suggests that the needles are nucleated by impurities or surface roughness.

XRD was used to determine whether the needles were associated with twinning around the (111) facet. We found no twins on a sample with a high density of needles. Furthermore, there was no broadening of the 422 reflection in samples with a high density of needles, showing that the crystalline structure of these layers was not degraded by the needles.

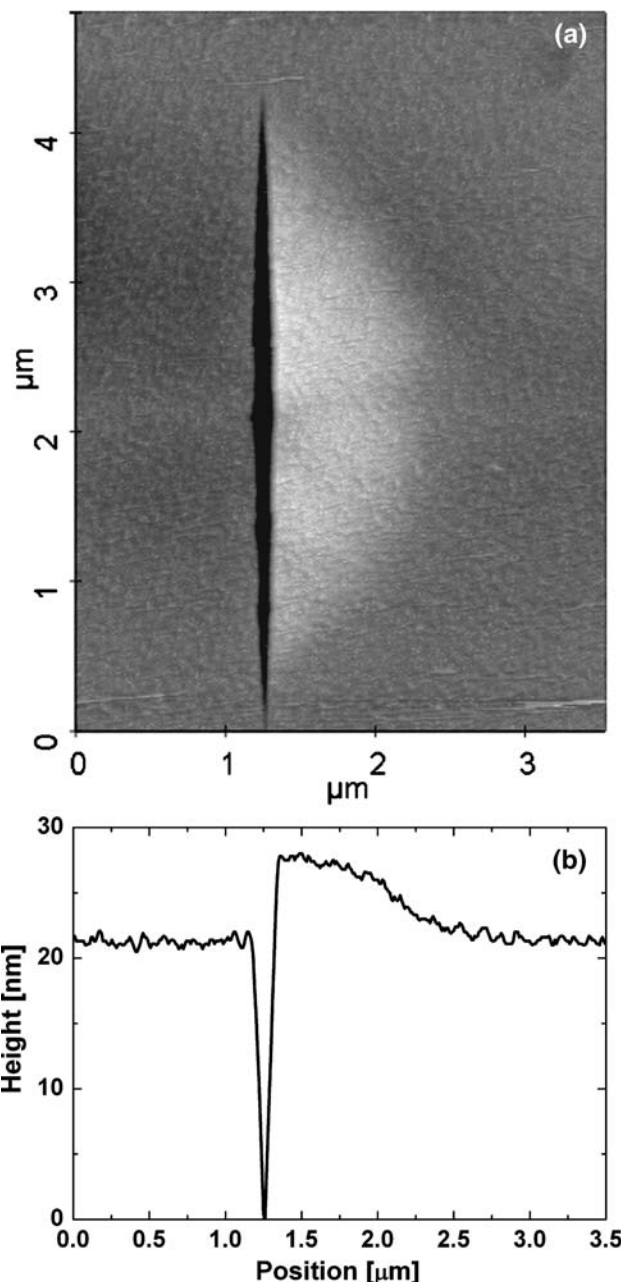

Fig. 8. (a) AFM image of a needle defect and (b) needle profile through the middle of the needle. The step-flow direction is toward the right.

We have suggested the following mechanism for needle formation: if the (111) facet forms on the surface due to, e.g., step poisoning by impurities the diffusion on this plane will not have a preferential direction. On the downstream side of the trench (left side of trench in Fig. 8) the surface is (211)B and the preferential direction of diffusion is toward the left,

away from the trench. This results in slightly less Te on the downstream side (left side) of the facet and a build-up on the upstream side of the trench. More details on needles can be found in Refs. 16 and 18. The absence of needles in HgTe suggests that cadmium occasionally temporarily disrupts the step-flow growth, resulting in the formation of a (111) facet.

Photoluminescence

The PL spectra in the CdHgTe layers consists of up to three overlapping peaks. The spectra at 11 K is shown in Fig. 9. The spectra are normalized to the peak with the highest intensity. Because the layers are of different compositions the spectra are shifted horizontally so that the high-energy peak from each layer lies at ΔEnergy = 0.

In some layers two peaks 10 ± 1 meV apart can clearly be observed. The PL FWHM increases significantly at T_{opt} + 5°C. Clearly, the presence of a high density of high-temperature voids results in an increased PL FWHM.

Our previous PL intensity versus excitation laser intensity measurements on CdHgTe layers have shown that the luminescence intensity of the peaks saturates at low temperatures.[24] This is in agreement with Lusson et al.[25] and indicates that the peaks are impurity related. Hg vacancies and n-type background doping are common in MBE-grown CdHgTe[1,2] and are most likely the origin of the PL peaks. The recombination is mainly nonradiative in the temperature range 60 K to 150 K.

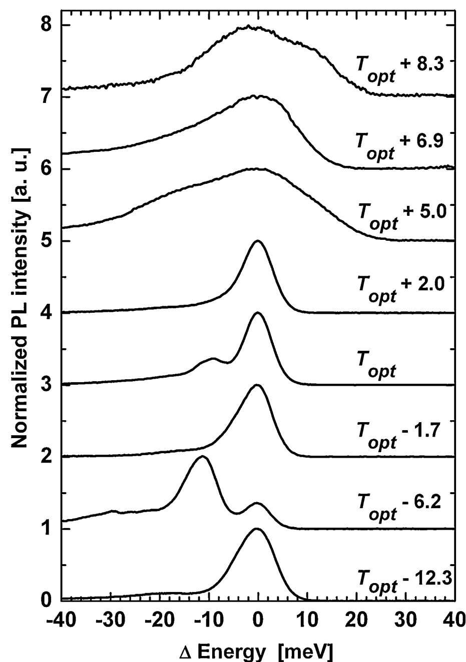

Fig. 9. PL spectra from the CdHgTe layers measured at 11 K. The spectra are shifted vertically for clarity. Because the layers are of different compositions the spectra are shifted horizontally so that the high-energy peak from each layer lies at ΔEnergy = 0.

Calculation of Optimal Growth Temperature for Other x-values

As mentioned above the optimal growth temperature in HgTe and $Cd_xHg_{1-x}Te$ was found to lie just below the Te-phase limit. The Te-phase limit is described by thermodynamics, and depends on the Hg flux (see the equation in Ref. 6). We have shown that the deviation from the Te-phase limit in HgTe can be determined from the microvoid shape and clustering in *just one* layer. When the Te-phase limit is known in HgTe then the Te-phase limit in Cd_xHg_{1-x} Te, at least in the x range of 0 to 0.50 which we have explored, can be calculated using thermodynamics. This is explained in more detail in Ref. 6 where we have shown experimentally that thermodynamics successfully predicts the onset of high-temperature voids. Thus, by growing just one HgTe layer and determining the Te-phase limit in HgTe, the optimal growth temperature in CdHgTe can be calculated.

Microvoids in Twin Domains of (111)B-oriented HgTe Films

A 3-μm-thick HgTe layer was grown on a 15-year-old 10×10 mm uncut (111)B-oriented CdZnTe substrate at T_{opt}. Microvoids are observed in the (111)B-oriented HgTe films in the form of equilateral triangles (Fig. 10), reflecting the symmetry of the (111) surface. The edges of the triangles are in the range of 0.8 μm to 1.1 μm and the depth is in the range of 160 nm to 500 nm, as measured by AFM. The edges are parallel to the $\langle 110 \rangle$ directions, which are consistent with {111} planes intersecting the

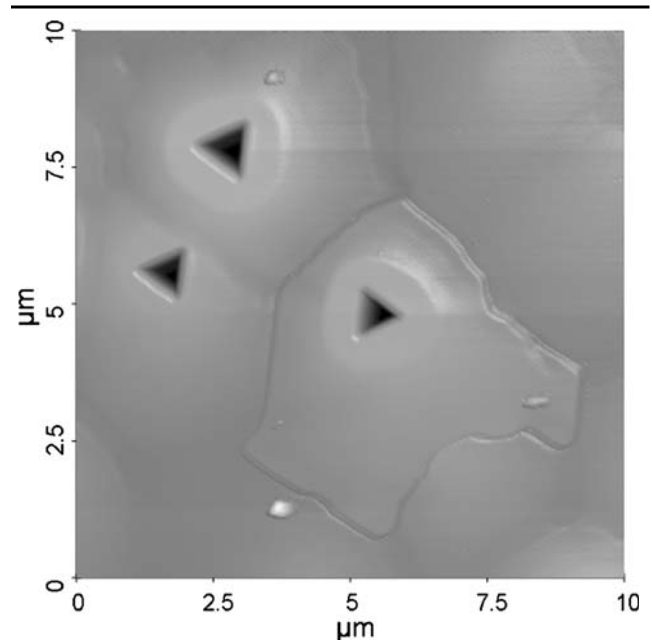

Fig. 10. AFM image of triangular microvoids in a (111)B-oriented unetched HgTe layer. The boundary around the microvoid to the right separates twinned and untwinned HgTe.

(111) surface. The slopes of the planes inside the microvoids have been measured with AFM and are often found to be consistent with {111} planes (within 5 deg). No direction-dependent build-up of material is observed on the (111)B surface. Very likely, this reflects the absence of step-flow growth on this orientation. Around the microvoids there is instead an approximately circular plateau with a diameter of 2.5 μm and a height of 12 nm above the surrounding (111) surface. These microvoids are similar in size and shape to the triangular pits reported by Hails et al.[26] in metalorganic vapor-phase epitaxy (MOVPE)-grown CdHgTe. The origin of the triangular microvoids in their layers was due to thermal etching during a short annealing procedure immediately following growth. Our layers were not annealed after growth, however.

Some microvoids were rotated 180 deg relative to the other microvoids. The rotated microvoids were enclosed by boundaries which could be observed in AFM as well as in Nomarski microscopy (Fig. 11a). To observe these boundaries more clearly we used a Hähnert and Schenk[8] etch. After a 45 s etch the contrast of the boundary surrounding the rotated microvoids was significantly enhanced (Fig. 11b). AFM profiles across the boundaries on etched and unetched layers (not shown) show that the etch attacked the boundary, resulting in a deeper and wider boundary after etch.

Tatsuoka et al.[27] have shown that triangular shapes on twinned (111)B-oriented CdTe layers were rotated 180 deg. Hails et al.[26] reported that twinning caused a 180 deg rotation of the triangular pits in CdHgTe. We used XRD to measure the content of twinned material in the film. This was performed by dividing the area of the 440 twin reflection by the sum of the area of the 440 twin reflection and 440 matrix reflection. This resulted in a twin content of 8%. The fractional area of the sample surface enclosed by the boundaries was measured from optical micrographs to be approximately 6%. In agreement with Hails et al. we therefore conclude that the rotation of the microvoids is due to twinning, which rotates the lattice by 180 deg. The boundaries observed around the rotated microvoids separate the twinned part of the layer from the untwinned part of the layer. The twin domains in this sample are irregularly shaped and are typically 3 μm wide.

CONCLUSIONS

We have shown how the shape and clustering of the microvoids in (211)B-oriented HgTe layers varies with growth temperature and how this variation can be used to determine the deviation from the optimal HgTe growth temperature. Furthermore, the optimal growth temperature in CdHgTe can be calculated using thermodynamics, once the optimal growth temperature in HgTe is known. Defect counts, 422 XRD FWHM, and PL spectra have been presented. We have found the optimal growth temperature to lie just below the Te-phase limit in HgTe and CdHgTe. A CdHgTe layer grown on an unsawn substrate exhibited an etch-pit density of 52,500 cm^{-2} which is close to the substrate etch-pit density.

PL spectra from CdHgTe samples grown 5°C or more above the optimal growth temperature display a broad FWHM. Apparently the high-temperature voids have a larger effect on the FWHM than the microvoids.

We have suggested that the formation mechanism for microvoids and needles in (211)B-oriented substrates can be explained by preferential Te surface diffusion. Microvoids in the twinned part of (111)B-oriented HgTe layers are rotated by 180 deg. The twin boundary can be clearly observed after a Hähnert and Schenk etch.

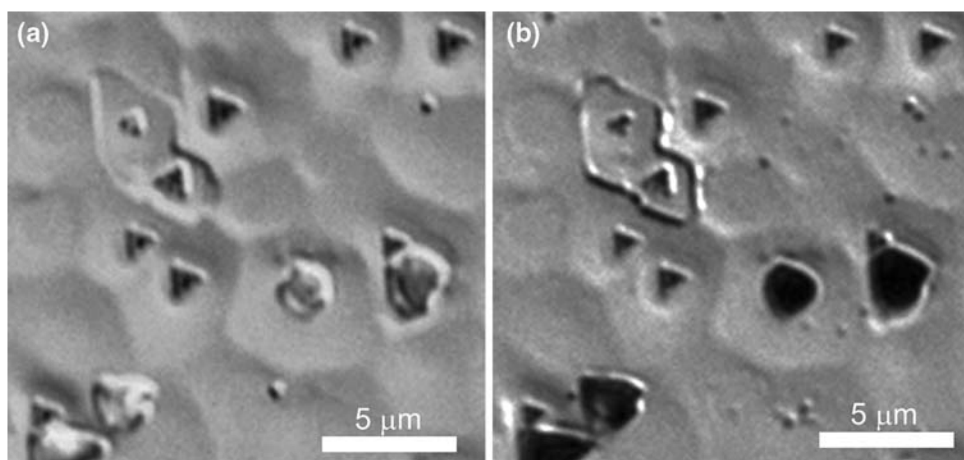

Fig. 11. Nomarski micrographs of triangular microvoids in (111)B-oriented HgTe. (a) As grown. (b) The same area after a 45 s Hähnert and Schenk etch.

ACKNOWLEDGEMENT

Laila Trosdahl-Iversen is acknowledged for substrate preparation and defect etching.

REFERENCES

1. R. Haakenaasen, H. Steen, T. Lorentzen, L. Trosdahl-Iversen, A.D. van Rheenen, and H. Syversen, *J. Electron. Mater.* 31, 710 (2002). doi:10.1007/s11664-002-0224-2.
2. R. Haakenaasen, H. Steen, E. Selvig, T. Lorentzen, A.D. van Rheenen, L. Trosdahl-Iversen, H. Syversen, D. Hall, and N. Gordon, *J. Electron. Mater.* 34, 922 (2005). doi:10.1007/s11664-005-0043-3.
3. G.L. Hansen, J.L. Schmit, and T.N. Casselman, *J. Appl. Phys.* 53, 7099 (1982). doi:10.1063/1.330018.
4. P.S. Wijewarnasuriya, M. Zandian, D.B. Young, J. Waldrop, D.D. Edwall, W.V. McLevige, D. Lee, and J. Arias, *J. Electron. Mater.* 28, 649 (1999). doi:10.1007/s11664-999-0048-4.
5. J.B. Varesi, A.A. Buell, J.M. Peterson, R.E. Bornfreund, M.F. Vilela, W.A. Radford, and S.M. Johnson, *J. Electron. Mater.* 32, 661 (2003). doi:10.1007/s11664-003-0049-7.
6. E. Selvig, C.R. Tonheim, K.O. Kongshaug, T. Skauli, T. Lorentzen, and R. Haakenaasen, *J. Vac. Sci. Technol. B* 25, 1776 (2007). doi:10.1116/1.2787876.
7. T. Skauli, T. Colin, and S. Løvold, *J. Vac. Sci. Technol. A* 12, 274 (1994). doi:10.1116/1.578867.
8. I. Hähnert and M. Schenk, *J. Cryst. Growth* 101, 251 (1990). doi:10.1016/0022-0248(90)90976-R.
9. I.V. Sabinina, A.K. Gutakovsky, Yu.G. Sidorov, and A.V. Latyshev, *J. Cryst. Growth* 274, 339 (2005). doi:10.1016/j.jcrysgro.2004.10.053.
10. Y. Chang, G. Badano, J. Zhao, C.H. Grein, S. Sivananthan, T. Aoki, and D.J. Smith, *Appl. Phys. Lett.* 83, 4785 (2003). doi:10.1063/1.1633017.
11. J.M. Arias, M. Zandian, J. Bajaj, J.G. Pasko, L.O. Bubulac, S.H. Shin, and R.E. De Wames, *J. Electron. Mater.* 24, 521 (1995). doi:10.1007/BF02657957.
12. E.C. Piquette, M. Zandian, D.D. Edwall, and J.M. Arias, *J. Electron. Mater.* 30, 627 (2001). doi:10.1007/BF02665846.
13. L.H. Zhang and C.J. Summers, *J. Electron. Mater.* 27, 634 (1998). doi:10.1007/s11664-998-0027-1.
14. T. Colin and T. Skauli, *J. Electron. Mater.* 26, 688 (1997). doi:10.1007/s11664-997-0217-2.
15. T. Colin (Ph.D. thesis, Université Joseph Fourier, Grenoble, 1991, in French).
16. E. Selvig, C.R. Tonheim, K.O. Kongshaug, T. Skauli, H. Hemmen, T. Lorentzen, and R. Haakenaasen, *J. Vac. Sci. Technol. B* 26, 525 (2008). doi:10.1116/1.2868782.
17. D. Chandra, H.D. Shih, F. Aqariden, R. Dat, S. Gutzler, M.J. Bevan, and T. Orent, *J. Electron. Mater.* 27, 640 (1998). doi:10.1007/s11664-998-0028-0.
18. R. Haakenaasen, H. Steen, E. Selvig, T. Lorentzen, A.D. van Rheenen, L. Trosdahl-Iversen, D. Hall, N. Gordon, T. Skauli, and A.H. Vaskinn, *Phys. Scripta* T126, 31 (2006). doi:10.1088/0031-8949/2006/T126/007.
19. L. Zhao, J.S. Speck, R. Rajavel, J. Jensen, D. Leonard, T. Strand, and W. Hamilton, *J. Electron. Mater.* 29, 732 (2000). doi:10.1007/s11664-000-0216-z.
20. J. Zhao et al., *J. Electron. Mater.* 33, 881 (2004). doi:10.1007/s11664-004-0215-6.
21. M. Zandian and E. Goo, *J. Electron. Mater.* 30, 623 (2001). doi:10.1007/BF02665845.
22. T. Nishiguchi, Y. Mukai, M. Nakamura, K. Nishio, T. Isshiki, S. Ohshima, and S. Nishino, *Mater. Sci. Forum* 457–460, 285 (2004).
23. Y. Chang, private communication.
24. M. Breivik, E. Selvig, C.R. Tonheim, E. Brendhagen, T. Brudevoll, A.D. van Rheenen, H. Steen, S. Nicolas, T. Lorentzen, and R. Haakenaasen, *J. Phys.: Conf. Ser.* 100, 042041. doi:10.1088/1742-6596/100/4/042041.
25. A. Lusson, F. Fuchs, and Y. Marfang, *J. Cryst. Growth* 101, 673 (1990). doi:10.1016/0022-0248(90)91056-V.
26. J.E. Hails, G.J. Russel, A.W. Brinkman, and J. Woods, *J. Cryst. Growth* 79, 940 (1986). doi:10.1016/0022-0248(86)90576-2.
27. H. Tatsuoka, H. Kuwabara, Y. Nakanishi, and H. Fujiyasu, *Appl. Surf. Sci.* 65/66, 426 (1993). doi:10.1016/0169-4332(93)90696-9.